Available online at www.sciencedirect.com
SCIENCE DIRECT®
Biomaterials 24 (2003) 3623–3631
Biomaterials
www.elsevier.com/locate/biomaterials

Structural and mechanical properties of the organic matrix layers of nacre

F. Song[a], A.K. Soh[b,*], Y.L. Bai[a]

[a] State Key Laboratory of Nonlinear Mechanics (LNM), Institute of Mechanics, Chinese Academy of Sciences, Beijing 100080, People's Republic of China

[b] Department of Mechanical Engineering, University of Hong Kong, Pokfulam Road, Hong Kong, People's Republic of China

Received 30 October 2002; accepted 12 March 2003

Abstract

The type of nanostructure referred to in biomineralization as a mineral bridge has been directly observed and measured in the organic matrix layers of nacre by transmission electron microscopy and scanning electron microscopy. Statistical analysis provides the geometric characteristics and a distribution law of the mineral bridges in the organic matrix layers. Experiments reveal that the nanostructures significantly influences the mechanical properties of the organic matrix layers. In addition, the mechanical analysis illustrates the effects of the nanostructures on the behaviors of the organic matrix layers, and the analytical results explain the corresponding experimental phenomena fairly well. The present study shows that the mineral bridges play a key role in the mechanical performances of the organic matrix layers of nacre. The results obtained provide a guide to the interfacial design of synthetic materials.

Keywords: Nacre; Mineral bridges; Nanostructures; Organic matrix; Mechanical property

1. Introduction

Nacre, or mother-of-pearl, is well known for its excellent mechanical properties, in particular, its high toughness, and it has, thus, become an attractive target for the design of toughened synthetic ceramics [1–4]. For example, the work of fracture of abalone nacre is about 3000 times greater than that of a single crystal of the pure mineral [5]. Previous studies showed that the main strengthening and toughening mechanisms of nacre are governed by its unique microarchitecture [6–8]. Conventionally, nacre is considered as a natural ceramic composite, the microarchitecture of which is described as a "brick and mortar" (BM) arrangement, where the bricks refer to flat polygonal crystals of aragonite and the mortar is a biological organic adhesive composed of polysaccharide and protein fibers. It is important to note that although the synthetic ceramics made of the same microarchitecture as that of nacre possess higher fracture toughness than those without nacre's microarchitecture, the former ceramics do not have a fracture toughness comparable to that of nacre [9]. These findings have led to further investigations on the microarchitecture and mechanical mechanisms of nacre.

Based on the "brick and mortar" arrangement of nacre, Schaffer et al. [10] reported their observations of the organic matrix layers of nacre by using atomic force microscope (AFM) and scanning ion conductance microscope (SICM). They pointed out that many nanopores in the interlamellar organic matrix sheets were taken out from the layers. Thus, they suggested that there might be a number of mineral bridges in the organic matrix layers of nacre and proposed a model in which nacre may be formed by continuous growth of mineral bridges through nanopores in organic matrix layers. Song et al. [11] confirmed the existence of mineral bridges in the organic matrix layers of nacre using transmission electron microscope (TEM), and proposed a distribution law of mineral bridges in the organic matrix layers by employing statistical methods.

To-date, many researchers have studied the mechanical behaviors of nacre focusing on the relationship

*Corresponding author. Tel.: +852-2859-8061; fax: +852-2858-5415.

E-mail address: aksoh@hkucc.hku.hk (A.K. Soh).

0142-9612/03/$ - see front matter © 2003 Elsevier Science Ltd. All rights reserved.
doi:10.1016/S0142-9612(03)00215-1

between the microarchitecture and mechanical properties. Currey [5] and Jackson et al. [7] studied the strengthening and toughening mechanisms of nacre. They proposed that the excellent performances of nacre were due to the BM arrangement, which gave rise to platelet pullout and organic matrix bridging. Sarikaya et al. [6] proposed that the main mechanisms of nacreous properties derived from the sliding of the platelets and the formation of organic ligaments between the layers. Wang et al. [8] showed that the toughness of nacre came from three mechanisms: crack deflection, platelet pullout and organic matrix bridging. More recently, Almqvist et al. [9] pointed out that ceramics laminated with organic materials possessed higher fracture resistance compared with non-laminated ceramics. However, synthetic materials made of interlocking ceramic tables bound by a few weight percent of ordinary adhesives did not have a toughness comparable to that of nacre. Subsequently, Smith et al. [12] felt that the key role to nacre's fracture resistance resided in the polymer adhesive of the organic matrix layers. However, the possible strengthening and toughening mechanisms have yet to be well understood.

In the present study, firstly, a TEM and a scanning electron microscope (SEM) are used to make various direct observations and an image analysis system (IAS) is employed to measure the mineral bridges in the organic matrix layers of nacre. Based on the measures, a statistical analysis is carried out to determine the geometric and distribution characteristics of the mineral bridges in the organic matrix layers of nacre. The present distribution law of mineral bridges accounts for the characteristic scales of the microarchitecture of nacre. The results are in good agreement with that described by Schaffer et al. [10]. Next, experimental observations are made to check whether the mineral bridges are able to prevent cracks from extending in the organic matrix layers of nacre. Finally, based on fracture mechanics and composite theories, some brief analyses are carried out to determine the effects of the mineral bridges on the mechanical properties of the organic matrix layers in nacre.

2. Experimental method

Samples made of the nacre of a *Haliotis iris* shell, which is an abalone shell from New Zealand, were used for testing. The keratin and prismatic layers of the shell were mechanically removed, and the residual part—i.e., the nacre of the shell—was washed using distilled water and air-dried at room temperature.

Microarchitectural observations of the nacre were performed using TEM (Hitachi H-8100) at an accelerating voltage of 200 kV. Thin films vertical to the surface of the shell, i.e., cross sections of the shell, were cut using a diamond saw, and that parallel to the surface of the shell were sliced off using a diamond knife. These two types of samples were then mechanically ground and thin-ion-beam milled, at an angle of 10°, to 50 μm thickness and, finally, perforated under a voltage of 5.5 kV. The microarchitectural and morphological images of the nacre were obtained and recorded by TEM and SEM (S-870), and all relevant data on the nacre were recorded using IAS (Image-Pro Plus 4.5, Media Cybernetics).

All mechanical tests of the nacre specimens were performed by carrying out three-point bending using an Instron 8562 machine, which was operated at a speed of 0.1 mm/min. The depth, width and length of each of the samples were 0.6, 2.5 and 14 mm, respectively. Note that the span of each of the samples was 10 mm. The narrow slot in each of the samples was introduced by a diamond saw. The samples prepared by employing the above methods were tested, and then observed and measured using TEM and IAS, respectively.

3. Results and discussions

3.1. Structural characteristics of organic matrix layers

First of all, the cross sections of nacre were directly observed using SEM and TEM. The morphologies of these cross sections revealed a traditional BM arrangement, as shown in Figs. 1a and b, consisting of a $CaCO_3$ (aragonite) platelet layer of 450–550 nm thick and an organic matrix (glycine- and alanine-rich protein and polysaccharide) layer of 21–31 nm thick. Thus, it was easy to estimate that the microarchitecture of the nacre coarsely contained 95 vol% of interlocking aragonite platelets staggered in successive laminae and separated by 5 vol% of organic matrix. However, the "mortar" of the nacre revealed a few nanoscale columns in the organic matrix layers, and the positions of those columns in the layers were random (refer to Fig. 1c). The aragonite columns, which are traditionally referred to as mineral bridges in biomineralization, passed through the mortar layers from one platelet to another and appeared to be roughly circular (refer to Fig. 1d). The diameter of the mineral bridges was measured to be 46 ± 8 nm, and the height of the mineral bridges of 26 ± 5 nm was equaled to the thickness of the organic matrix layers of the nacre.

Next, the aragonite platelet surfaces of nacre, which are parallel to the surface of the shell, were studied by SEM and TEM. Some independent regions were randomly chosen on the surfaces of the nacre (refer to Fig. 2a). By measuring the areas of the regions and the numbers of the platelets in the regions, the average area A of each aragonite platelet on the surfaces was calculated to be approximately 16 m^2. Since each perfect

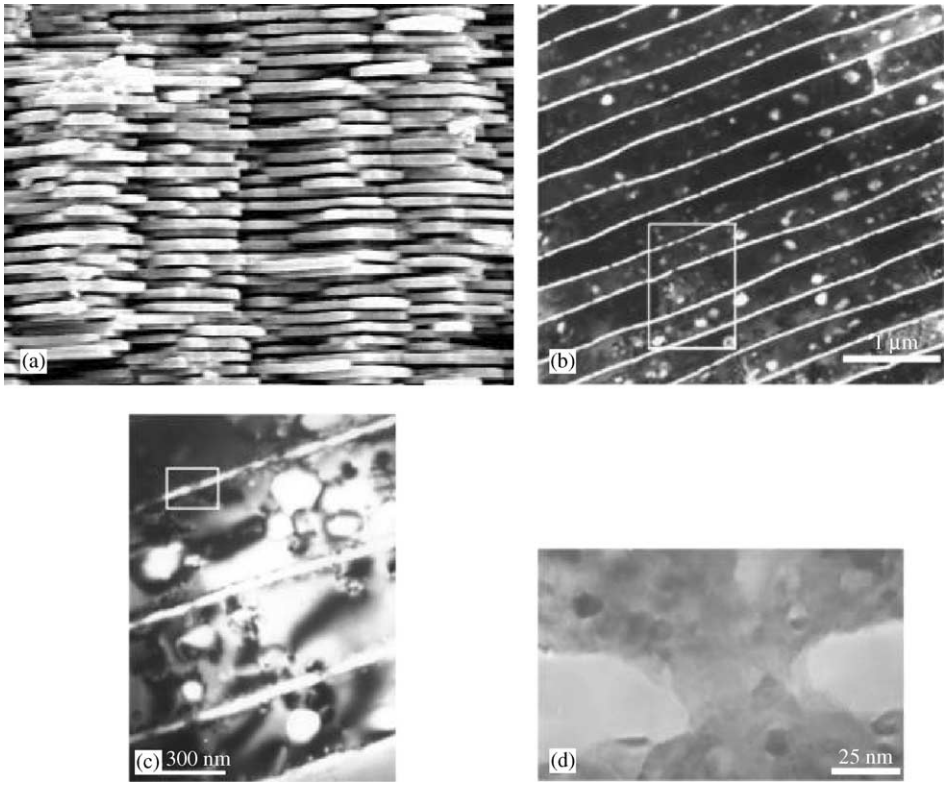

Fig. 1. (a) SEM micrograph showing the cross section of nacre as "brick and mortar" structure. (b) TEM micrograph showing the microstructure of the cross section of nacre, which appears to be a traditional "brick and mortar" arrangement. (c) (the boxed area in (b)) TEM micrograph showing some mineral bridges in the organic matrix layers of nacre. The mineral bridges are randomly arranged in the layers. (d) (the boxed area in (c)) TEM micrograph showing a mineral bridge between two successive platelets of nacre. The appearance of the mineral bridges is more or less like circular column.

platelet on the surfaces could be roughly described as a hexagon [5,8,10], the average side length and the average diagonal length of each platelet were approximately computed as $l_S = 2.5\,\mathrm{m}$ and $l_D = 5\,\mu\mathrm{m}$, respectively. Furthermore, some mineral bridges and nanopores could be observed directly in the interlamellar organic matrix sheets on the surfaces (refer to Figs. 2b and c). Note that the nanopores were at the residual positions where the mineral bridges were pulled out from the sheets. These mineral bridges and nanopores were randomly arranged in the interlamellar organic matrix sheets, and the diameters of the bridges and pores were 36–54 and 5–50 nm, respectively. The average diameter of the nanopores clearly was less than that of the mineral bridges; this might be due to the expansion of the organic matrix once the mineral bridges have been pulled out.

To investigate the distribution characteristics of the mineral bridges in the mortar layers, several independent fields were randomly selected in the interlamellar organic matrix sheet of the nacre parallel to the surface of the shell (refer to the boxed area in Fig. 2b). By measuring both the numbers of the mineral bridges and nanopores in each field, together with the areas of the fields, the average density of the mineral bridges on the surfaces was determined to be $105 \pm 15\,\mathrm{m}^{-2}$. Based on this result, the average number of mineral bridges in the interlamellar organic matrix sheet on each aragonite platelet was calculated to be 1680 ± 240.

Six cross sections of nacre were chosen stochastically; these cross sections contained 60 perfect aragonite platelets. Fig. 3a shows a histogram, which was obtained by measuring the length and the number of these platelets, in which the length of the platelets, measured to be $l \pm 0.50\,\mathrm{m}$ ($l = 1, 2, \ldots, 7$), was roughly attributed to the l-value of the horizontal coordinates. From the histogram, the average length of the platelets on the cross sections was approximately determined to be $l_0 = 4\,\mathrm{m}$. Fifteen platelets on the cross sections of lengths $4 \pm 0.2\,\mathrm{m}$ were then chosen for counting the number of mineral bridges, and the data obtained is presented in Fig. 3b. The total number of mineral bridges for the 15 platelets on the cross sections was 602. Therefore, the average number of mineral bridges in each platelet was $N_x \approx 40$; the average linear density of the mineral bridges was $\rho_0 \approx N_x/l_0 = 10\,\mathrm{m}^{-1}$.

From the present statistical analysis, the relevant characteristics of the mineral bridges on each platelet could also be determined: For example, the average density and number of mineral bridges were

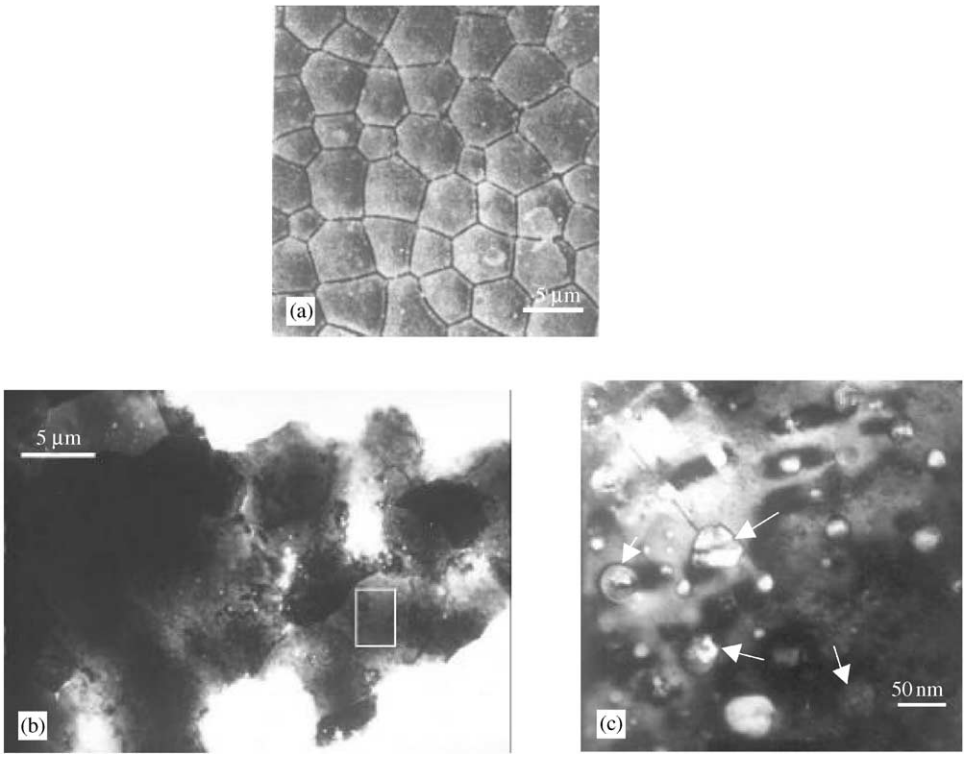

Fig. 2. (a) SEM micrograph showing the platelet surface of nacre parallel to the surface of the shell. Each aragonite platelet on the surfaces is roughly similar to a hexagon. (b) TEM image of the aragonite platelet surface of nacre. There is a thin organic matrix layer containing glycine- and alanine-rich protein and polysaccharide on the surface. (c) (the boxed area in (b)) TEM image of mineral bridges (see arrows) and pores (the other white parts) in the organic matrix layer (dark parts) on a platelet surface. The mineral bridges and pores are randomly positioned on the surface.

$n_0 \approx 100\,\mathrm{m}^{-2}$ and $N \approx 1600$, respectively. These results are in rough agreement with those measured directly earlier.

Furthermore, each of the chosen 15 platelets was divided into 16 equal units, along the direction of the organic matrix layer. By separately adding the number of mineral bridges (on the 15 platelets) contained by each unit, a histogram of the number of mineral bridges on the platelets was obtained, as shown in Fig. 3c. The average value and standard deviation computed from the histogram are $\mu = 2\,\mathrm{m}$ and $\sigma = 0.67\,\mathrm{m}$, respectively. The histogram indicates that the distribution of mineral bridges on each aragonite platelet was heterogeneous. After normalization, the histogram approximately represents the average distribution of the number of mineral bridges for each of the platelets, along the length of the platelet itself, on the cross sections. A curve can be used to approximate the histogram (refer to Fig. 3c). The curve representing the linear density of the number of mineral bridges in each platelet on the cross section of the nacre can be expressed as

$$\rho(x) = 2\rho_0 \exp\left[-V_p \frac{l_0}{l_D}\left(x - \frac{l_0}{2}\right)^2\right], \tag{1}$$

where $x (0 \leqslant x \leqslant l_0)$ is the local coordinate from one end of a given platelet to an arbitrary point in the platelet itself, on the cross section; $V_p = 0.95$ is the volume fraction of aragonite platelet in the nacre.

From Eq. (1), the average bridge-to-bridge spacing between the neighboring bridges for each platelet is

$$\langle s \rangle_{\text{whole}} = \int_0^{l_0} x\rho(x)\,\mathrm{d}x \approx 80\,\text{nm}. \tag{2}$$

In addition, from Eq. (1), we obtain

$$\int_{\mu-\sigma}^{\mu+\sigma} \rho(x)\,\mathrm{d}x = 0.68 N_x. \tag{3}$$

Eq. (3) illustrates a feature of the distribution of the mineral bridges, i.e., a central region exists along the length of each platelet, on the cross sections, in which the number of mineral bridges is 68% of that on a platelet. The local coordinates of the central region are $(\mu - \sigma, \mu + \sigma) = (1.33, 2.67)$, and the length of the central region, 1.34 m, is approximately equal to one-third of the average length of the platelets on the cross sections. In the central region, the average bridge-to-bridge spacing between the neighboring mineral bridges is

$$\langle s \rangle_{\text{center}} = \int_{\mu-\sigma}^{\mu+\sigma} x\rho(x)\,\mathrm{d}x \approx 50\,\text{nm}. \tag{4}$$

Eq. (4) shows that the average density of the mineral bridges in the central region is higher than that in the whole platelet.

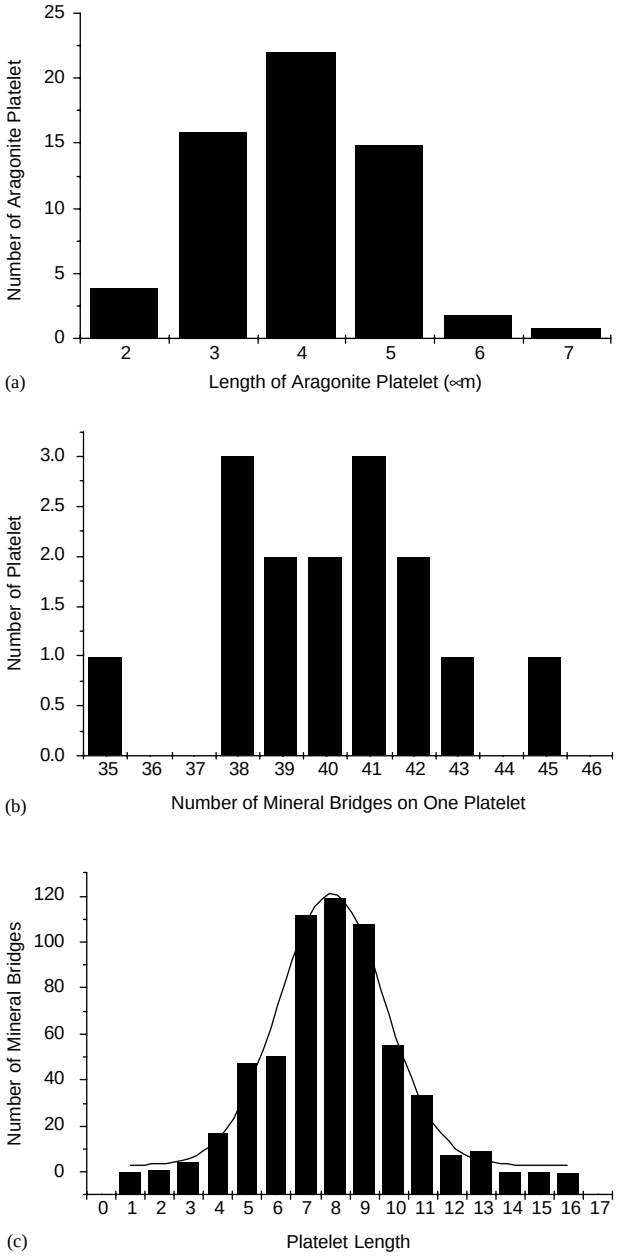

Fig. 3. (a) Histogram of the length of 30 platelets on the cross sections of the nacre. This distribution illustrates that the average length of one platelet on the cross sections is approximately equal to 4 μm. (b) Histogram of the number of mineral bridges of each of the thirty platelets on the cross sections of the nacre. It shows that the total number of mineral bridges of the platelets is 1169, and the average number of mineral bridges of each platelet on the cross section is approximately equal to 40. (c) Histogram of the distribution of the number of mineral bridges along the length of platelet on the cross sections. The distribution reveals that most of the mineral bridges are concentrated in the central region of the platelet.

The distribution characteristics of the mineral bridges described above are only true for a cross section of the nacre. However, these results can be extended to each perfect platelet of the nacre. This is because the structures of all cross sections of the nacre are statistically the same, and the distributions of the mineral bridges are statistically independent of the cross sections. In accordance with Eq. (1), the joint distribution density of the number of mineral bridges on each perfect platelet can be approximated as

$$n(x,y) = \rho(x)\rho(y) = 4n_0 \exp\left\{-V_p \frac{l_0}{l_D}\left[\left(x-\frac{l_0}{2}\right)^2+\left(y-\frac{l_0}{2}\right)^2\right]\right\}, \quad (5)$$

where $n_0 = \rho_0^2$ denotes the average density of the mineral bridges on the platelet surface, and x and $y (0 \leqslant x, y \leqslant l_0)$ are local coordinates, the origin of which is one end of the platelet on the cross section. Eq. (5) yields

$$\int_{\mu-\sigma}^{\mu+\sigma}\int_{\mu-\sigma}^{\mu+\sigma} n(x,y)\,dx\,dy \approx 0.46N. \quad (6)$$

Eq. (6) indicates that each platelet surface of nacre has a central region, in which the number of mineral bridges is 46% that of the whole platelet. The area of the central region is coarsely determined to be one-ninth that of the whole platelet. The average density of the mineral bridges on the central region is about $414\,m^{-2}$ (refer to Fig. 4).

In general, the microarchitecture of nacre can be approximately described as a hypo-periodic structure, i.e., on the surfaces of the nacre parallel to that of the shell, each periodic element is a hexagonal aragonite platelet with average side length l_S or diagonal length l_D; and on the cross sections, each periodic element is an aragonite platelet with average length l_0 coupled with the organic matrix layer on it.

Similar to the case of the diameter and the distribution of mineral bridges in the organic matrix layers, the above results are in good agreement with those reported by Schaffer et al. [10]. It is important to note that the present distributions of mineral bridges, as given by Eqs. (1) and (5), are different from those expressions given in Ref. [11]. The present distributions include the characteristic scales ($V_p l_0/l_D$ and l_0) of nacre and the average densities (ρ_0 and n_0) of mineral bridges in the organic matrix layers in order to represent the structural characteristics of nacre more accurately.

3.2. Mechanical properties of organic matrix layers

To analyze the effects of mineral bridges on the mechanical behaviors of the organic matrix layers of the nacre, consider an interlamellar organic matrix sheet corresponding to just a platelet, which is one periodic element of nacre, as shown in Fig. 4. Obviously, due to the existence of mineral bridges, this sheet possesses anisotropic properties. For convenience, the sheet is approximated as a square with average length, l_0, for its cross section such that l_0^2 is the same as the average area

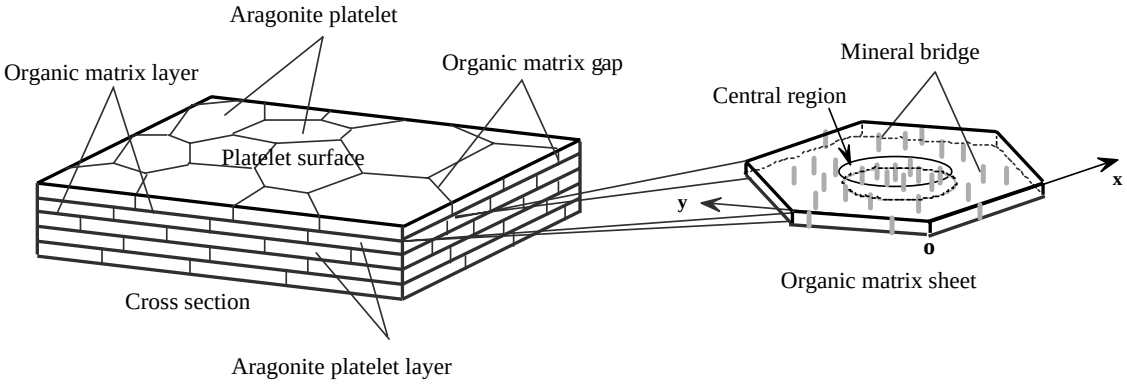

Fig. 4. Schematic illustration showing the "brick and mortar" microarchitecture of nacre, the mineral bridges in an organic matrix sheet and the coordinate system on the cross section.

of one platelet. From the above study, we estimate that total cross-sectional area of the mineral bridges in the sheet is about 2.7 μm^2, which is approximately one-sixth of the area of each platelet. The organic matrix sheet is coarsely treated as a fiber-reinforced composite, which consists of an organic matrix and fibers of mineral bridges. Based on the distribution law of the mineral bridges in the organic matrix layers given by Eq. (5), the volume fraction of the fibers along the side of the sheet is defined as

$$V_f|_{l_1}^{l_2} = \frac{\pi D^2}{4 l_0 (l_2 - l_1)} \int_{l_1}^{l_2} \left(\int_0^{l_0} n(x, y)\, dy \right) dx, \tag{7}$$

where (l_1, l_2) denotes a given region on the side of the sheet in the local x-direction satisfying the essential condition, $l_0 \geqslant l_2 - l_1 \geqslant dx \geqslant D$, in which $D = 46$ nm is the average diameter of the mineral bridges, x and y $(0 \leqslant x, y \leqslant l_0)$ are the local coordinates of the sheet. Obviously, the volume fraction of the organic matrix in the same region is $V_m|_{l_1}^{l_2} = 1 - V_f|_{l_1}^{l_2}$.

From Eq. (7), the average volume fraction of the mineral bridges in the interlamellar organic matrix sheet and in its central region are determined to be $V_f|_0^{l_0} = 0.17$ and $V_f|_{\mu-\sigma}^{\mu+\sigma} = 0.35$, respectively, where $(\mu - \sigma, \mu + \sigma)$ denotes the coordinates of the central region of the sheet on the cross section of the nacre.

3.2.1. Young's modulus of organic matrix layers

In accordance with the composite theory [13], the average Young's modulus of the sheet in the direction of the mineral bridges within the region (l_1, l_2) can be expressed as

$$E_c|_{l_1}^{l_2} = E_m \left(1 + 24 V_f|_{l_1}^{l_2}\right), \tag{8}$$

where $E_m = 4$ GPa and $E_f = 100$ GPa [7] are Young's moduli of the organic matrix and the mineral bridges, respectively. Note that Young's modulus of the latter is deemed to be the same as that of aragonite platelet. When the existence of mineral bridges is not considered in Eq. (8), we have $V_m|_{l_1}^{l_2} = 1$ and $V_f|_{l_1}^{l_2} = 0$. This equation is, thus, reduced to $E_c|_{l_1}^{l_2} = E_m$, which is the traditional Young's modulus of the organic matrix layers of nacre. In contrast, when the existence of mineral bridges is considered, the average Young's modulus of the organic matrix layers is determined to be $E_c|_0^{l_0} = 5E_m$ for the whole sheet, in particular, $E_c|_{\mu-\sigma}^{\mu+\sigma} = 9.4E_m$ for the central region of the sheet. These results indicate that the mineral bridges significantly increase Young's modulus of the organic matrix layers of nacre in the direction of the mineral bridges.

To validate Young's modulus of the organic matrix layers studied above, we employ Riley's model [14] as follows:

$$E_{nacre} = V_p E_p \left[1 - \frac{\ln(u+1)}{u}\right] + (1 - V_p) E_o \tag{9}$$

and

$$u = s\sqrt{\frac{M V_p}{E_p (1 - V_p)}}, \tag{10}$$

where s is the aspect ratio; E_p, E_o and E_{nacre} are Young's moduli of the platelet, organic matrix layers and nacre, respectively; and M the shear modulus of organic matrix. With $s = 8$, $V_p = 0.95$, $E_p = 100$ GPa and $M = 4.6$ GPa [7], and by assuming $E_o = E_c|_0^{l_0} = 5E_m$, E_{nacre} is determined to be 68.9 GPa. This Young's modulus of nacre is in good agreement with that of 70 GPa measured experimentally by Jackson et al. [7].

3.2.2. Fracture toughness of organic matrix layers

One of the outstanding properties of nacre is its high toughness. To further examine the effects of mineral bridges on the interfacial fracture toughness of nacre, fracture tests of nacre were carried out by using the three-point bending method, as shown in Fig. 5a. It has been found that a crack can only propagate in the organic matrix layers or gaps of the nacre, as shown in Fig. 5b. On the cross section of the nacre, when a crack

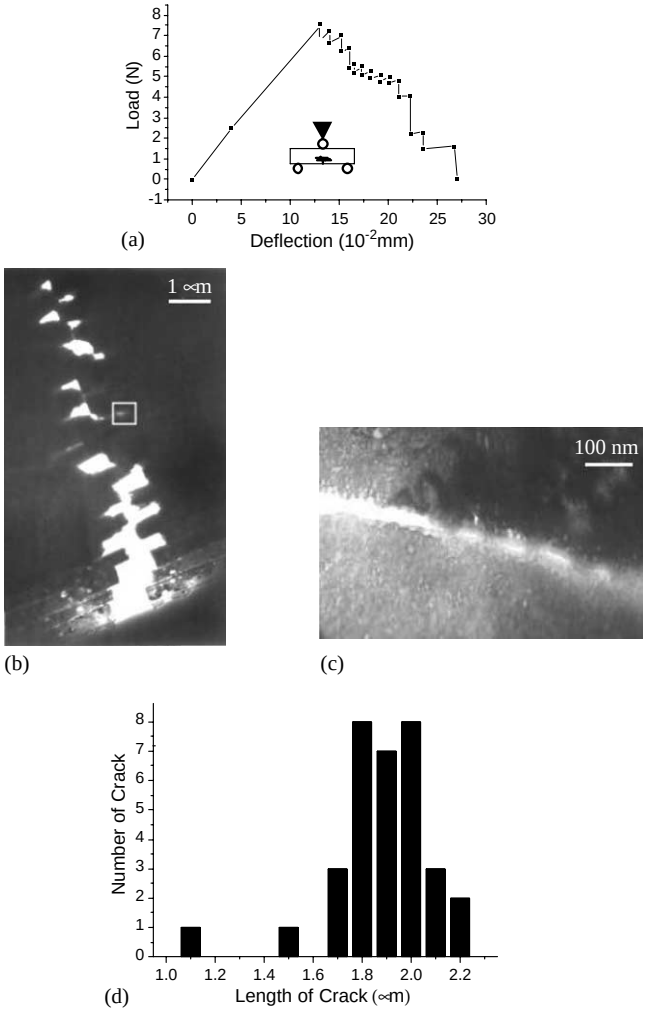

Fig. 5. (a) Three-point bending test curve of nacre. (b) TEM micrograph showing the fracture surface morphology on the cross section of the nacre. It indicates that a crack propagates in the organic matrix layers or gaps of the nacre. (c) (enlarged view of the boxed area in (b)) TEM micrograph showing the mineral bridges that hinder crack propagation in an organic matrix layer. (d) Histogram of the length of 33 cracks in the samples tested by three-point bending, the direction of which is all along the organic matrix layer on the cross sections. This distribution illustrates that the average length of the cracks in each of the organic matrix layers is approximately equal to $1.88 \pm 0.20\,\mu m$.

was deflected from an organic matrix gap to an organic matrix layer, the crack traveled in the layer in two opposite directions. The two tips of the crack propagated separately in the organic matrix layer for a distance before being arrested by the mineral bridges (refer to Fig. 5c). The distance of travel of the two crack tips were approximately equal in each of the organic matrix layers, and on the average, each crack tip traveled pass one organic matrix gap of the above platelet layer. With the increase of the applied load, a new crack tip was formed in the gap of the next platelet layer. This crack tip rapidly passed through the gap to the next organic matrix layer. Fig. 5c shows that when a crack propagated into a region of an organic matrix layer of the nacre, some mineral bridges of the region would prevent the crack from further development in the layer. In particular, on the path of the crack propagation, the organic matrix between successive platelets was broken, and the link between the platelets was just the mineral bridges. Therefore, in the field near the crack tip, the mineral bridges instead of the organic adhesive of the nacre plays the main role in withstanding the external load. It is an indication that at the interfaces of the nacre the following relation is satisfied

$$\sigma_m \leqslant \sigma_c \leqslant \sigma_f, \tag{11}$$

where σ_m, σ_f and σ_c are the fracture strength of the organic matrix, the mineral bridge and the organic matrix sheet presented above, respectively.

The average traveling distance of each crack tip in the organic matrix layers was measured and statistically determined to be $1.88 \pm 0.20\,\mu m$ (refer to Fig. 5d). Based on the structure of the organic matrix layers, there was an indication that the crack propagation was stopped in the central region of the mineral bridges situated in the organic matrix layers of the nacre.

The organic matrix sheet presented above is employed to analyze the experimental observations. Based on fracture mechanics [15], when a crack extends from l_1 to $l_2 = l_1 + dl$ in the sheet, the incremental work for fracture of the organic matrix is

$$dW_m = 2\gamma_m(1 - V_f|_{l_1}^{l_2}) l_0\, dl. \tag{12}$$

The incremental work for fracture of the mineral bridges is

$$dW_f = 2\gamma_f V_f|_{l_1}^{l_2} l_0\, dl \tag{13}$$

and the incremental work for fracture of the interfaces between the organic matrix and mineral bridges is

$$\begin{aligned} dW_{mf} &= 2\gamma_m \left(\pi D t \frac{4 l_0\, dl}{\pi D^2} V_f|_{l_1}^{l_2} \right) \\ &\approx 2\gamma_m \frac{116}{46} V_f \Big|_{l_1}^{l_2} l_0\, dl, \end{aligned} \tag{14}$$

where γ_m and γ_f are the fracture surface energy of the organic matrix and the mineral bridges, respectively. In Eq. (14), $t = 26\,nm$ is the average height of the mineral bridges and $t \approx 29D/46$ is employed. Therefore, using Eqs. (12)–(14), the crack resistance of the region, (l_1, l_2), can be expressed as

$$\begin{aligned} R_c|_{l_1}^{l_2} &= \frac{1}{l_0} \frac{d(W_m + W_f + W_{mf})}{dl} \\ &\approx (1 + 1.5 V_f|_{l_1}^{l_2}) R_m, \end{aligned} \tag{15}$$

where $R_m = 2\gamma_m$ denotes the crack resistance of the sheet without the mineral bridges. Note that γ_f/γ_m is deemed a small value and, therefore, it is omitted in the equation. From Eq. (15), we obtain $R_c|_{l_1}^{l_2} = R_m$ when the

nanostructures are not considered, $R_c|_0^{l_0} \approx 1.25R_m$ for the whole sheet and $R_c|_{\mu-\sigma}^{\mu+\sigma} \approx 1.51R_m$ for the central region.

Based on the Irwin's relation, the fracture toughness of the sheet is written as

$$K_{Ic}^c|_{l_1}^{l_2} = K_{Ic}^m \sqrt{\left(1 + 24V_f|_{l_1}^{l_2}\right)\left(1 + 1.5V_f|_{l_1}^{l_2}\right)}, \quad (16)$$

where $K_{Ic}^m = \sqrt{E_m R_m}$ is the fracture toughness of organic matrix. When the mineral bridges in the sheet are not considered, we have $K_{Ic}^c|_{l_1}^{l_2} = K_{Ic}^m$, which is the traditional fracture toughness of the organic matrix layers of nacre. However, when the mineral bridges are considered, the average fracture toughness is $K_{Ic}^c|_0^{l_0} \approx 2.5K_{Ic}^m$ in the whole sheet, and $K_{Ic}^c|_{\mu-\sigma}^{\mu+\sigma} \approx 3.7K_{Ic}^m$ in the central region of the sheet. Obviously, the mineral bridges effectively increase the crack resistance and the fracture toughness of the organic matrix layers of nacre (refer to Fig. 6).

These results illustrate that when a crack is propagating towards the central region, the crack resistance and the fracture toughness of the organic matrix layer is rapidly increased. Therefore, the crack is arrested in the central region. Since there are no mineral bridges in the organic matrix gaps of the nacre, in general, the fracture strength of the gap is less than that of the central region. When the applied load is increased, the crack has to form a new tip at a gap of the neighboring platelet layer. The crack will then pass through the gap to the next organic matrix layer. There is a clear indication that the mineral bridges cause deflection of the crack. Fig. 6 shows the crack resistance and fracture toughness encountered in a periodic element on the cross section of an organic matrix layer of nacre. As far as the whole nacre is concerned, its fracture toughness is not only the sliding of the aragonite platelets and the formation of organic ligaments between the platelet layers [6], but also the result of two main mechanisms acting in concert, i.e., crack deflection and platelet pullout [7,8]. However, each of the toughening mechanisms is intimately associated with the organic matrix layers of the nacre, of course, with the mineral bridges in the layers.

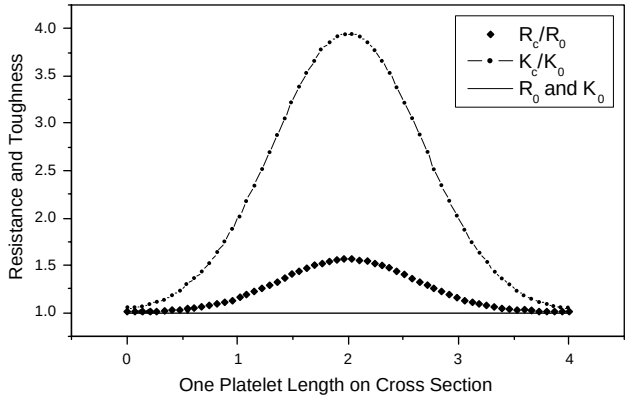

Fig. 6. Plots showing the crack resistance and fracture toughness over one platelet element on the cross section of nacre. The horizontal line stands for the crack resistance and fracture toughness of the organic matrix layers without the mineral bridges; the median and the upper curves denote the crack resistance and the fracture toughness of the layer with the mineral bridges, respectively.

Furthermore, the effects of the mineral bridges on the extended length of the crack propagating in an organic matrix layer are studied. In accordance with the theory of linear elastic fracture mechanics [15], the condition for arresting of crack is

$$G|_0^{a_{cp}} - R_c|_0^{a_{cp}} = 0, \quad (17)$$

where a_{cp} is the crack length at which the crack is arrested, $G|_0^x = (\pi\sigma_\infty^2 x)/E_c|_0^x$ is the crack extended force and σ_∞ is the external force. Substituting Eq. (15) into this condition, and noticing the fracture strength of the organic matrix $K_{Ic}^m = \sigma_m\sqrt{\pi a_{op}}$ and Eq. (11), we obtain

$$\frac{a_{cp}}{a_{op}} \leqslant \frac{1 + 1.5V_f|_0^{a_{cp}}}{1 + 24V_f|_0^{a_{cp}}}, \quad (18)$$

where a_{op} is the crack length at which the crack is arrested in the organic matrix layer without mineral bridges. By approximating the average volume fraction of the mineral bridges as, $V_f|_0^{l_0} = 0.17$, Eq. (18) yields $4a_{cp} \leqslant a_{op}$. This shows that the average length of the crack extension in an organic matrix layer without mineral bridges is more than four times of that in an organic matrix layer of nacre. This may explain why in the fracture process, delaminated states hardly happened in nacre.

4. Conclusions

Based on direct observations and statistical analyses, the existence of mineral bridges of nacre has been confirmed, and the approximate distribution of the mineral bridges in the organic matrix layers has been obtained. Furthermore, the excellent performances of nacre are proven to be intimately associated with the mineral bridges in the organic matrix interfaces of the nacre itself. From the viewpoint of biomimetic design, nacre is an ideal layered ceramic composite. The organic matrix layers are weak interfaces relative to the aragonite layers in nacre. Therefore, the existence of mineral bridges reinforces the weak interfaces such that the interfaces become just suitable for the crack to extend in itself. Perhaps, this explains why the interfaces of synthetic layered materials are not as strong as those of nacre. In addition, the present study shows that the microarchitecture of nacre should be referred to as a "brick–bridge–mortar" (BBM) arrangement, instead of a traditional "brick–mortar" arrangement. Since the crystallographic orientations of 3–10 successive platelets remain the same [16], it is reasonable to suggest that the

microarchitecture of nacre is, to some extent, a tangled BBM structure.

Acknowledgements

This work was supported by the National Natural Science Foundations of China (Grant.10072067) and the Research Grants Council of the Hong Kong Special Administrative Region, China (Project No. HKU 7086/02E).

References

[1] Heuer AH, et al. Innovative materials processing strategies: a biomimetic approach. Science 1992;255:1098–105.
[2] Stupp SI, Braun PV. Molecular manipulation of microstructure: biomaterials, ceramics, and semiconductors. Science 1997;277:1242–8.
[3] Addadi L, Weiner S. A pavement of pearl. Nature 1997;389:912–5.
[4] Kaplan DL. Mollusc shell structure: novel design strategies for synthetic materials. Curr Opin Solid St M 1998;3:232–6.
[5] Currey JD. Mechanical properties of mother of pearl in tension. Proc R Soc London B 1977;196:443–63.
[6] Sarikaya M, Liu J, Aksay IA. Nacre: properties, crystallography, morphology, and formation. In: Sarikaya M, Aksay IA, editors. Biomimetics: design and processing of materials. New York: Woodbury, 1995. p. 35–90.
[7] Jackson AP, Vincent JFV, Turner RM. The mechanical design of nacre. Proc R Soc London B 1988;234:415–40.
[8] Wang RZ, Wen HB, Cui FZ, Zhang HB, Li HD. Observations of damage morphologies in nacre during deformation and fracture. J Mater Sci 1995;30:2299–304.
[9] Almqvist N, et al. Methods for fabricating and characterizing a new generation of biomimetic materials. Mater Sci Eng C 1999;7:37–43.
[10] Schaffer TE, et al. Does abalone nacre form by heteroepiaxial nucleation or by growth through mineral bridges? Chem Mater 1997;9:1731–40.
[11] Song F, Zhang XH, Bai YL. Microstructure and characteristics of the organic matrix layers of nacre. J Mater Res 2002;17:1567–70.
[12] Smith BL, et al. Molecular mechanistic origin of the toughness of natural adhesives, fibres and composites. Nature 1999;399:761–3.
[13] Piggott MR. Load-bearing fibre composites. Oxford: Pergamon Press, 1980.
[14] Lusis J, Woodhams RT, Xanthos M. The effects of flake aspect ratio on the flexural properties of mica reinforced plastics. Polym Eng Sci 1973;13:139–45.
[15] Broek D. Elementary engineering fracture mechanics. The Hague: Martinus Nijhoff, 1982.
[16] Feng QL, et al. Crystal orientation toughening mechanisms and a mimic of nacre. Mater Sci Eng C 2000;11:19–25.